Structural Engineering and Mechanics, Vol. 24, No. 6 (2006) 741-764
DOI: http://dx.doi.org/10.12989/sem.2006.24.6.741

Time-dependent analysis of launched bridges

M. Mapelli†

SPEA Ingegneria Europea, Via Vida 11, 20127 Milan, Italy

F. Mola‡ and M. A. Pisani‡†

Department of Structural Engineering, Politecnico di Milano, Piazza Leonardo da Vinci 32, 20133 Milan, Italy

(Received February 25, 2005, Accepted July 11, 2006)

Abstract. The time-dependent analysis of prestressed concrete bridges built adopting the incremental launching technique is presented. After summarizing the well known results derived from the elastic analysis, the problem is approached in the visco-elastic domain taking into account the effects consequent to the complex load history affecting the structure. In particular, the effects produced by prestressing applied both in the launching phase and after it and by application of imposed displacements and of delayed restraints during the launching phases are carefully investigated through a refined analytical procedure. The reliability of the proposed algorithm is tested by means of comparisons with reference cases for which exact solutions are known. A case study of general interest is then discussed in detail. This case study demonstrates that a purely elastic approach represents a too crude approximation, which is unable to describe the specific character of the problem.

Keywords: prestressed concrete bridges; creep; launched bridges.

1. Introduction

The procedure of incremental launching for prestressed concrete bridges was developed in the sixties when jacking operations and the construction of sliding supports able to minimize friction forces became possible. The incremental launching technique can be profitably used for bridges with straight axis and nearly constant spans ranging between 40 m and 70 m (Leonhardt 1973, Grant 1975, Baur 1977). Nevertheless, bridges with circular axis of small curvature in the horizontal plane have been recently constructed (Favre and Laurencet 1999).

In order to justify the extra cost due to the need of special launching devices, the adoption of this construction system can be recommended when the number of the spans is quite large. This condition, together with other prerequisites (i.e., the constancy of the transverse section and an optimum value of the length/weight ratio for the spans) gives to launched bridges a typical configuration.

† H.O. Technical Support to Engineer's Representative
‡ Professor
‡† Associate Professor, Corresponding author, E-mail: pisani@stru.polimi.it

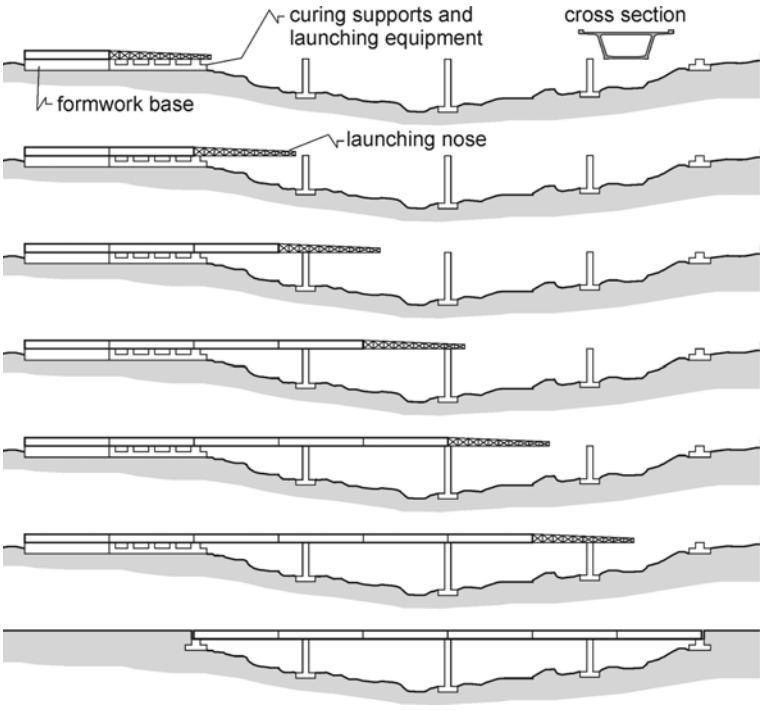

Fig. 1 Construction phases

The constructional process starts with the concreting of the first segment (15~30 m long) by using a formwork base placed beyond an abutment. The subsequent operations consist in the launching of the bridge step by step when new segments are added to the bridge tail (see Fig. 1). Therefore, the structure is affected by rheological inhomogeneity along its axis and the structural scheme continuously varies during the launching phases. Special care has to be devoted to the correct evaluation of the transverse displacements and of their variation during these phases as they influence the geometric tolerance and affect the final configuration of the bridge, the moment distribution and the values of the support reactions.

In the last three decades many theoretical works have been devoted to the investigation of the structural behaviour of launched bridges, and many practical aspects have been solved in order to control the bridge behaviour during the construction process. The most important problems are related to the state of stress and deformation affecting the two spans located behind the advancing edge of the bridge. When the head of the bridge reaches a support, the span located beyond the support behaves as a cantilever which can exhibit a length equal to the one of the bridge spans in the final configuration. For bridges with constant central spans the negative moment acting in the cantilever can attain a value many times larger in comparison with the one affecting the internal spans, which exhibit the statical behaviour of a continuous beam. Feasible choices to reduce the bending moment in the cantilever consist in reducing their length by introducing provisional supports or stays (see for instance Rosignoli 1998, 1999, 2000, Göhler and Pearson 2000, Hewson 2003, Sasmal *et al*. 2004). A second option consists in reducing the weight of the cantilever span by adding a steel nose. The first option induces a significant increase of the construction cost.

Moreover, the insertion of provisional stays presents substantial difficulties as a consequence of the uncertainties connected to the stays prestressing, to thermal effects and to possible mankind errors. For these reasons, the most popular solution for reducing the bending moment in the cantilever consists in applying a light metallic nose at the bridge head.

A large part of the theoretical studies have been oriented to the analysis of the structural system including the prestressed concrete bridge deck and its metallic nose. The most interesting results achieved in these studies regard the structural optimization in terms of bending moment and transverse displacement distribution. Optimization can be obtained by prescribing feasible values for the ratios between the weight, the length and the flexural stiffness of the nose and the cantilevered part. Another problem studied in depth regards the definition of the most feasible profile of the prestressing tendons. Owing to the alternate presence of negative and positive bending moments in the transverse sections of the bridge deck during the launching process, the most feasible prestressing in this phase is a centric one. In this way no transverse displacements are induced by prestressing. In the final configuration, in which the structural behaviour is that of a continuous beam, an additional prestressing tendon with variable profile, capable of maximizing the prestressing effects, has to be provided.

The analyses performed in the aforementioned studies assume a linear elastic behaviour for the materials. This approach is generally sufficient for steel bridges and for composite steel-concrete bridges in which the concrete slab is cast when the steel beams have reached their final configuration.

When prestressed concrete bridges are dealt with, however, the elastic analysis represents only a rough approximation because the delayed deformation of concrete strongly affects the structural behaviour both in the construction phases and in the final configuration. The most outstanding problems related to creep and shrinkage of concrete in launched bridges are the rheological inhomogeneity of the structure, the introduction of delayed restraints, the time development of stress redistribution in the transverse sections and the time variation of the state of deformation of the structure, as discussed by Ghali and Favre (1986).

In the present study the complex problem now briefly discussed is investigated and solved in the linear visco-elastic domain. The analysis develops through three basic steps. The first step regards the formulation of the sectional analysis, assuming as unknowns the parameters of the plane section deformation, when internal actions (variable in time) are applied. The second step regards structural analysis devoted to deduce the compatibility equations by means of the principle of virtual work. Finally, the resulting system of equations is solved. The constitutive laws of the various segments of the bridge deck are expressed in integral form, according to Mc Henry Principle of Superposition (Mc Henry 1943), so that the problem is governed by a set of Volterra integral equations. Therefore, a complex numerical algorithm is adopted to evaluate the structural behaviour of the bridge during the construction phases and under service loads.

Some applications to simple problems (for which exact solution is known) are firstly discussed in order to evaluate the accuracy of the proposed numerical algorithms. The analysis of an eight span prestressed concrete box girder bridge is then discussed in detail. This case study allows the marked influence exerted by the delayed deformation of concrete on the structural response of prestressed concrete launched bridges to be pointed out.

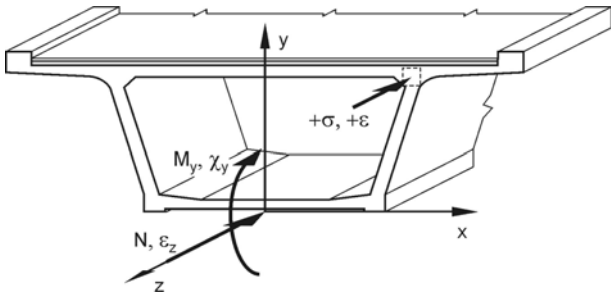

Fig. 2 Convention showing sense in which stress, strain and load components are considered positive

2. Assumptions

The analytical formulation adopts the following assumptions:

1. any bridge deck cross-section consists of steel elements and one single concrete casting that is the only visco-elastic material inside that cross-section;
2. when dealing with a composite steel-concrete bridge deck (i.e., stiffened plate prestressed composite sections, see for instance Rosignoli 1998), the local effects of longitudinal slip at the interface between steel and concrete due to deformation of the shear connectors is neglected;
3. reinforcing bars and steel tendons are perfectly bonded to the surrounding concrete. This means that external prestressing is not taken into account;
4. prestressing is carried out in two phases: launch prestressing (usually centroidal) is carried out during incremental launch, whereas service prestressing is carried out upon completion of the launch;
5. a linear visco-elastic constitutive law is adopted for concrete. This assumption means that concrete is not cracked both during launch and under service loads;
6. the deck axis is straight and the vertical axis y of every cross section is an axis of symmetry (see Fig. 2);
7. the long-term loads and prestressing act in the symmetry plane y-z;
8. the bridge has spans of variable length, whereas the monolithic segments have constant length (constant launching span).

3. Cross-sectional analysis

Mola (1986) carried out the analysis of the heterogeneous cross-section by means of the solving kernels matrix algorithm and of the equilibrium method. An application of this approach was worked out in Mola and Pisani (1993). Following the same logic the equilibrium method will be adopted in the following to take into account the time evolution of stresses and strains due to internal actions and prestressing.

3.1 Compatibility equations

Owing to the hypothesis that the y-z plane is a plane of symmetry of the cross section, Bernoulli-

Navier assumption may be expressed as:

$$\varepsilon(x, y, z, t) = \varepsilon_z(z, t) + \chi(z, t) \cdot y = \underline{\rho}^T \underline{\psi}(z, t) \tag{1}$$

where:

$$\underline{\rho}^T = |1 \quad y| \; ; \; \underline{\psi}(z, t) = |\varepsilon_z(z, t) \quad \chi(z, t)|^T \tag{2}$$

$\varepsilon_z(z, t)$ is the longitudinal strain measured in the origin of the x and y axes, and $\chi(z, t)$ is the curvature in the y-z plane (see Fig. 2).

The vectors:

$$\underline{\rho}_{si}^T = |1 \quad y_{si}| \; ; \; \underline{\rho}_{pj}^T = |1 \quad y_{pj}| \tag{3}$$

fix the ordinate of the i-th reinforcing bar (subscript s) and of the j-th prestressing tendon (subscript p).

From the hypotheses of perfect bond (assumptions 2 and 3) it follows that:

$$\begin{aligned} \varepsilon_c(y, z, t) &= \underline{\rho}^T \underline{\psi}(z, t) \\ \varepsilon_a(y, z, t) &= \underline{\rho}^T \underline{\psi}(z, t) \\ \varepsilon_{si}(z, t) &= \underline{\rho}_{si}^T \underline{\psi}(z, t) \\ \varepsilon_{pj}(z, t) &= \varepsilon^*(y_{pj}, z, t) + \bar{\varepsilon}_{pj}(z) \end{aligned} \tag{4}$$

where subscript c stands for concrete and subscript a refers to rolled steel (in composite steel-concrete cross sections and in the launching nose).

In the fourth of Eqs. (4) $\bar{\varepsilon}_{pj}(z)$ is the non-compatible strain between the prestressing tendon and the surrounding concrete imposed by stressing, and $\varepsilon^*(y_{pj}, z, t)$ is the strain increase that develops in the concrete at the level of the j-th prestressing tendon between time t_{pj}^- immediately before stressing and the actual time t:

$$\varepsilon^*(y_{pj}, z, t) = \varepsilon(y_{pj}, z, t) - \varepsilon(y_{pj}, z, t_{pj}^-) \tag{5}$$

In matrix notation Eq. (5) becomes:

$$\varepsilon_{pj}(z, t) = \underline{\rho}_{pj}^T \underline{\psi}^*(z, t) + \bar{\varepsilon}_{pj}(z) = \underline{\rho}_{pj}^T [\underline{\psi}(z, t) - \underline{\psi}(z, t_{pj}^-)] + \bar{\varepsilon}_{pj}(z) \tag{6}$$

The adoption of the prestrain $\bar{\varepsilon}_{pj}(z)$ (see Eibl 1995) to take into account prestressing needs a clarification: when dealing with post-tensioning, this non-compatible strain is the sum of the elongation of the tendon and the shortening of the surrounding concrete, that is:

$$\bar{\varepsilon}_{pj}(z) = \bar{\varepsilon}_{j\text{-th tendon}}(z) - \bar{\varepsilon}_c(y_{pj}, z) \tag{7}$$

The elongation of the tendon at stressing $\bar{\varepsilon}_{j\text{-th tendon}}(z)$ (i.e., the strain in the tendon immediately

before grouting) can be easily evaluated once that the stress resultant at the stressing jack is known and the friction losses along the tendon up to the cross-section under consideration has been computed. The relaxation of the prestressing steel is usually included in this term.

Because of the lack of bond between the tendons and the concrete substructure before grouting, in this phase the tendons can be replaced by an equivalent load (see for instance Libby 1984). Term $\overline{\varepsilon}_c(y_{pj}, z)$ is the elastic strain caused in the concrete substructure, in the cross-section under consideration, at $y = y_{pj}$ by this equivalent load.

3.2 Equilibrium equations

The equilibrium equations of the cross-section under consideration are:

$$\int_{A_c} \sigma_c(y,z,t) \cdot \underline{\rho} \cdot dA_c + \int_{A_a} \sigma_a(y,z,t) \cdot \underline{\rho} \cdot dA_a + \sum_i A_{si} \cdot \sigma_{si}(z,t) \cdot \underline{\rho}_{si} + \sum_j A_{pj} \cdot \sigma_{pj}(z,t) \cdot \underline{\rho}_{pj} = \underline{M}(z,t) \tag{8}$$

with $\underline{M}^T(z,t) = \left| N(z,t) \;\; M_y(z,t) \right|$ vector of the internal actions.

3.3 Constitutive laws

Because of the assumption (5), the constitutive laws of the materials involved in the analysis can be written as follows:

$$\varepsilon_c(y,z,t) = \sigma_c(y,z,t_0) \cdot J(t,t_0) + \int_{t_0}^{t} d_\tau \sigma_c(y,z,\tau) \cdot J(t,\tau) + \varepsilon_{sh}(z,t) \tag{9}$$

$$\begin{aligned} \sigma_a(x,y,z,t) &= \varepsilon_a(x,y,z,t) \cdot E_a \\ \sigma_{si}(z,t) &= \varepsilon_{si}(z,t) \cdot E_s \\ \sigma_{pj}(z,t) &= \varepsilon_{pj}(z,t) \cdot E_p \end{aligned} \tag{10}$$

where $J(t, t_0)$ is the creep function of concrete, t_0 is its age at first loading, t is its actual age, $\varepsilon_{sh}(z,t)$ is the shrinkage strain and $d_\tau \sigma_c(y,z,\tau) = \dfrac{\partial \sigma_c(y,z,\tau)}{\partial \tau} d\tau$ where τ is the integration variable.

The progress of the construction phases because of incremental launching together with the rheological behaviour of concrete demand the adoption of a time-scale. The time-scale adopted in Eq. (9) is the age of concrete. To simplify the computations, the age of concrete inside each monolithic segment of the bridge deck will therefore be adopted all over section 3 to describe the evolution of internal actions, stresses and strain in every cross-section inside that monolithic segment.

3.4 Instantaneous change $\Delta\underline{\psi}$ of vector $\underline{\psi}$

Every instantaneous change of the internal action in the cross section at time t_k because of a phase of launch, because of the application of the service prestressing, or because of an increase of the

dead load, forces us to compute the corresponding change $\Delta_k \underline{\psi}(z) = \underline{\psi}(z, t_k) - \underline{\psi}(z, t_k^-)$ of vector $\underline{\psi}(z, t)$.

In this case Eq. (9) becomes:

$$\Delta\sigma_c(y, z, t_k) = E_c(t_k) \cdot \Delta\varepsilon_c(y, z, t_k) \tag{11}$$

where $E_c(t_k)$ is the Young modulus of concrete at age t_k.

Substituting Eqs. (11) and (10) into Eq. (8) and then Eqs. (4) and (1) in the outcome one obtains:

$$[\underline{\underline{B}}_c(z, t_k) + \underline{\underline{B}}_s^{(k)}(z)] \cdot \Delta_k \underline{\psi}(z) = \Delta_k \underline{M}(z) + \Delta \underline{\overline{P}}_k(z) \tag{12}$$

where

$$\underline{\underline{B}}_c(z, t_k) = E_c(t_k) \int_{A_c(z)} \underline{\rho}\,\underline{\rho}^T dA_c(z) \tag{13}$$

is the stiffness matrix of the concrete part of the cross-section,

$$\underline{\underline{B}}_s^{(k)}(z) = E_a \int_{A_a(z)} \underline{\rho} \cdot \underline{\rho}^T dA_a(z) + E_s \sum\nolimits_i A_{si} \cdot \underline{\rho}_{si} \cdot \underline{\rho}_{si}^T + E_p \sum\nolimits_j^{(k)} A_{pj} \cdot \underline{\rho}_{pj} \cdot \underline{\rho}_{pj}^T \tag{14}$$

is the stiffness matrix of the steel part of the cross section (that takes into account both the tendons that are stressed at time t_k and all the tendons stressed in former times), and

$$\Delta \underline{\overline{P}}_k(z) = -E_p \sum\nolimits_n A_{pn}\, \underline{\rho}_{pn}\, \overline{\varepsilon}_{pn}(z) \tag{15}$$

is the vector that determines the internal action equivalent to prestressing due only to the tendons that are stressed at time t_k.

Vector $\Delta_k \underline{M}(z)$ stands for the vector of the internal actions due to the external loads and to the reaction of the constraints. This means that $\Delta_k \underline{M}(z)$ includes also the bending moment that results from the deformation of the structure during prestressing.

It is important to point out that $\Delta_k \underline{M}(z)$ depends on the overall instantaneous behaviour of the redundant structure and therefore it is an unknown.

3.5 Delayed variation $\delta\underline{\psi}$ of vector $\underline{\psi}$

Mc Henry superposition principle applies because of assumption 5. Therefore, vector $\underline{\psi}(z, t)$ (i.e., the vector that describes the strain all over the cross-section by means of Eqs. (1) and (4)) consists in two stepwise functions, the instantaneous change $\Delta\underline{\psi}$ and continuous variation $\delta\underline{\psi}$ between the events of elastic instantaneous nature:

$$\underline{\psi}(z, t) = \sum_{r=1}^{k-1} [\Delta_r \underline{\psi}(z) + \delta_r \underline{\psi}(z, t_{r+1}^-)] + \Delta_k \underline{\psi}(z) + \delta_k \underline{\psi}(z, t) \qquad t_k < t < t_{k+1} \tag{16}$$

The time-intervals between these instantaneous events (i.e., the interval between time t_r and time t_{r+1} in Eq. (16)) will be named phases because they correspond to the construction phases. Superscript - means the instant immediately before the instantaneous change. In Eq. (16), the actual time t is inside the k-th phase.

If a prestressing tendon has been stressed at time $t_{pj} = t_n$, that is at the beginning of the n-th phase, from Eq. (6) it follows that

$$\underline{\psi}^*(z,t) = \underline{\psi}(z,t) - \underline{\psi}(z,t_n^-) \tag{17}$$

Substituting Eq. (16) into Eq. (17) one obtains:

$$\underline{\psi}^*(z,t) = \sum_{r=1}^{k-1}[\Delta_r\underline{\psi}(z) + \delta_r\underline{\psi}(z,t_{r+1}^-)] + \Delta_k\underline{\psi}(z) + \delta_k\underline{\psi}(z,t) - \sum_{r=1}^{n-1}[\Delta_r\underline{\psi}(z) + \delta_r\underline{\psi}(z,t_{r+1}^-)]$$

$$= \sum_{r=n}^{k-1}[\Delta_r\underline{\psi}(z) + \delta_r\underline{\psi}(z,t_{r+1}^-)] + \Delta_k\underline{\psi}(z) + \delta_k\underline{\psi}(z,t) \tag{18}$$

Because of Eqs. (16), (17) and (18), the compatibility equations in the k-th phase become:

$$\begin{aligned}
\varepsilon_c(y,z,t) - \varepsilon_c(y,z,t_k) &= \underline{\rho}^T \cdot \delta_k\underline{\psi}(z,t) \\
\varepsilon_a(y,z,t) - \varepsilon_a(y,z,t_k) &= \underline{\rho}^T \cdot \delta_k\underline{\psi}(z,t) \\
\varepsilon_{si}(z,t) - \varepsilon_{si}(z,t_k) &= \underline{\rho}_{si}^T \cdot \delta_k\underline{\psi}(z,t) \\
\varepsilon_{pj}(z,t) - \varepsilon_{pj}(z,t_k) &= \underline{\rho}_{pj}^T \cdot \delta_k\underline{\psi}(z,t)
\end{aligned} \qquad t_k < t < t_{k+1} \tag{19}$$

Moreover, because of Eq. (9), the stress variation in the r-th phase contributes to the strain variation at time t in the k-th phase ($t_k < t < t_{k+1}$; $k \geq r$) according to the following expression (see Fig. 3):

$$\begin{aligned}
\delta_k\varepsilon_c(y,z,t) &= \varepsilon_c(y,z,t) - \varepsilon_c(y,z,t_k) = \\
&= \sum_{r=1}^{k-1}\left\{\Delta_r\sigma_c(y,z)\cdot[J(t,t_r) - J(t_k,t_r)] + \int_{t_r}^{t_{r+1}} d_\tau\sigma_c(y,z,\tau)\cdot[J(t,\tau) - J(t_k,\tau)]\right\} + \\
&+ \Delta_k\sigma_c(y,z)\cdot[J(t,t_k) - J(t_k,t_k)] + \int_{t_k}^{t} d_\tau\sigma_c(y,z,\tau)\cdot J(t,\tau) + [\varepsilon_{sh}(z,t) - \varepsilon_{sh}(z,t_k)]
\end{aligned} \tag{20}$$

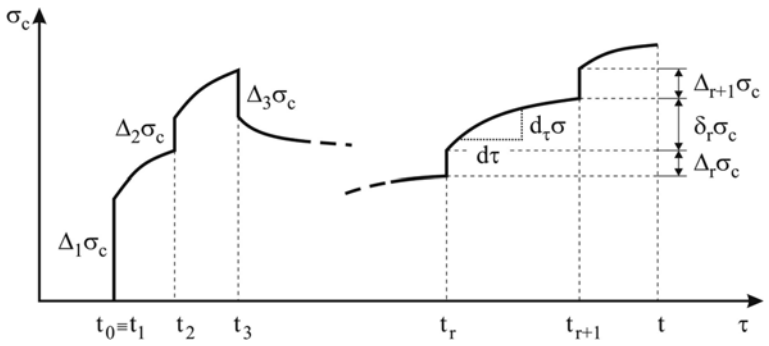

Fig. 3 Time evolution of the stress in concrete

Substituting Eq. (20) in the first of Eqs. (19) one obtains:

$$\begin{aligned}\underline{\underline{A}}(z)\cdot\delta_k\underline{\psi}(z,t) &= \sum_{r=1}^{k}\left\{\int_{A_c(z)}\Delta_r\sigma_c(y,z)\cdot[J(t,t_r)-J(t_k,t_r)]\cdot\underline{\rho}\cdot dA_c(z)\right\}+\\ &+\sum_{r=1}^{k-1}\left\{\int_{A_c(z)}\int_{t_r}^{t_{r+1}}d_\tau\sigma_c(y,z,\tau)\cdot[J(t,\tau)-J(t_k,\tau)]\cdot\underline{\rho}\cdot dA_c(z)\right\}+\\ &+\int_{A_c(z)}\int_{t_k}^{t}d_\tau\sigma_c(y,z,\tau)\cdot J(t,\tau)\cdot\underline{\rho}\cdot dA_c(z)+\\ &+\int_{A_c(z)}[\varepsilon_{sh}(z,t)-\varepsilon_{sh}(z,t_k)]\cdot\underline{\rho}\cdot dA_c(z)\end{aligned}\tag{21}$$

where:

$$\underline{\underline{A}}(z)=\int_{A_c(z)}\underline{\rho}\,\underline{\rho}^T dA_c(z)=\int_{A_c(z)}\begin{vmatrix}1 & y\\ y & y^2\end{vmatrix}dA_c(z)=\begin{vmatrix}A_c(z) & S_{yc}(z)\\ S_{yc}(z) & I_{yyc}(z)\end{vmatrix}=\underline{\underline{B}}_c(z,t)\cdot\frac{1}{E_c(t)}\tag{22}$$

Replacing the first of Eqs. (4) in Eq. (11), pre-multiplying both members of the latter by $[J(t,t_r)-J(t_k,t_r)]\cdot\underline{\rho}$ and then integrating over area $A_c(z)$ gives a new expression for the first term of the right-hand member of Eq. (21):

$$\int_{A_c(z)}\Delta_r\sigma_c(y,z)\cdot[J(t,t_r)-J(t_k,t_r)]\cdot\underline{\rho}\cdot dA_c(z)=E_c(t_r)\cdot\underline{\underline{A}}(z)\cdot\Delta_r\underline{\psi}(z)\cdot[J(t,t_r)-J(t_k,t_r)]\tag{23}$$

The partial derivative of the equilibrium Eq. (8) with respect to time τ is:

$$\begin{aligned}&\int_{A_c(z)}d_\tau\sigma_c(y,z,\tau)\cdot\underline{\rho}\cdot dA_c(z)+\int_{A_a(z)}d_\tau\sigma_a(y,z,\tau)\cdot\underline{\rho}\cdot dA_a(z)+\\ &+\Sigma_i d_\tau\sigma_{si}(z,\tau)A_{si}\underline{\rho}_{si}+\Sigma_j^{(k)}d_\tau\sigma_{pj}(z,\tau)A_{pj}\underline{\rho}_{pj}=d\underline{M}(z,\tau)\end{aligned}\tag{24}$$

This equation, together with the constitutive laws of reinforcing bars, tendons and rolled steel, and with the compatibility equations allows the third term of the right-hand member of Eq. (21) to be written as follows:

$$\begin{aligned}&\int_{A_c(z)}\int_{t_k}^{t}d_\tau\sigma_c(y,z,\tau)\cdot J(t,\tau)\cdot\underline{\rho}\cdot dA_c(z)=\int_{t_k}^{t}J(t,\tau)\int_{A_c(z)}d_\tau\sigma_c(y,z,\tau)\cdot\underline{\rho}\cdot dA_c(z)=\\ &=\int_{t_k}^{t}J(t,\tau)\cdot\Big[d\underline{M}(z,\tau)-\int_{A_a(z)}\underline{\rho}\cdot d_\tau\sigma_a(y,z,\tau)\cdot dA_a(z)-\Sigma_i\underline{\rho}_{si}\cdot d\sigma_{si}(z,\tau)\cdot A_{si}+\\ &\qquad-\Sigma_j^{(k)}\underline{\rho}_{pj}\cdot d\sigma_{pj}(z,\tau)\cdot A_{pj}\Big]=\\ &=\int_{t_k}^{t}J(t,\tau)\cdot d\underline{M}(z,\tau)-\underline{\underline{B}}_s^{(k)}(z)\cdot\int_{t_k}^{t}J(t,\tau)\cdot d\underline{\psi}(z,\tau)\qquad t_k<t<t_{k+1};\quad t_k<\tau<t\end{aligned}\tag{25}$$

Similarly, the second term of the right-hand member of Eq. (21) becomes:

$$\begin{aligned}&\int_{A_c(z)}\int_{t_r}^{t_{r+1}}d_\tau\sigma_c(y,z,\tau)\cdot[J(t,\tau)-J(t_k,\tau)]\cdot\underline{\rho}\cdot dA_c(z)=\qquad t_k<t<t_{k+1}\\ &=\int_{t_r}^{t_{r+1}}[J(t,\tau)-J(t_k,\tau)]\cdot d\underline{M}(z,\tau)-\underline{\underline{B}}_s^{(r)}(z)\int_{t_r}^{t_{r+1}}[J(t,\tau)-J(t_k,\tau)]\cdot d\underline{\psi}(z,\tau)\quad t_r<\tau<t_{r+1}\end{aligned}\tag{26}$$

Therefore, Eq. (21) may be written as follows:

$$\frac{\underline{\underline{B}}_c(z,t)}{E_c(t)}\delta_k\underline{\psi}(z,t)+\underline{\underline{B}}_s^{(k)}(z)\cdot\int_{t_k}^{t}J(t,\tau)d\underline{\psi}(z,\tau)=\sum_{r=1}^{k}\{\underline{\underline{B}}_c(z,t_r)\cdot\Delta_r\underline{\psi}(z)\cdot[J(t,t_r)-J(t_k,t_r)]\}+$$

$$-\sum_{r=1}^{k-1}\underline{\underline{B}}_s^{(r)}(z)\cdot\int_{t_r}^{t_{r+1}}[J(t,\tau)-J(t_k,\tau)]d\underline{\psi}(z,\tau)+\sum_{r=1}^{k-1}\int_{t_r}^{t_{r+1}}[J(t,\tau)-J(t_k,\tau)]d\underline{M}(z,\tau)+ \tag{27}$$

$$+\int_{t_k}^{t}J(t,\tau)\cdot d\underline{M}(z,\tau)+[\underline{D}_{sh}(z,t)-\underline{D}_{sh}(z,t_k)]$$

where

$$\underline{D}_{sh}(z,t)=\varepsilon_{sh}(z,t)\cdot\int_{A_c(z)}\underline{\rho}\cdot dA_c(z)=\varepsilon_{sh}(z,t)\cdot\left|A_c(z)\;\;S_{yc}(z)\right|^T \tag{28}$$

Eq. (27) is a system of two Volterra integral equations. The unknowns are the terms of vector $\delta_k\underline{\psi}(z,t)=\left|\delta_k\varepsilon_z(z,t)\;\;\delta_k\chi_y(z,t)\right|^T$ that describes the strain variation in the k-th phase.

It is important to point out that Eq. (27) takes into account the instantaneous changes $\Delta_r\underline{M}(z)$ through $\Delta_r\underline{\psi}(z)$ (because of Eq. (12)):

$$\Delta_r\underline{\psi}(z)=[\underline{\underline{B}}_c(z)+\underline{\underline{B}}_s^{(r)}(z)]^{-1}\cdot[\Delta_r\underline{M}(z)+\Delta\overline{\underline{P}}_r(z)] \tag{29}$$

The solution of Eq. (27) can be achieved only by means of numerical integration, due to the complexity of the creep function of concrete. The method adopted is a Gauss quadrature formula (see Pisani 1994) with two sampling points inside each time-step. This method allows more refined results in comparison with the ones obtainable by assuming the trapezoidal rule (Bazant 1975).

The k-th phase (between time t_k and time t_{k+1}) is subdivided in time-steps, according to the following rule (see CEB 1984):

$$t_{s+1,k}=(t_{s,k}-t_{1,k})\times 10^m+t_{1,k}\qquad s=2,\ldots,NS_k$$

$$t_{2,k}-t_{1,k}=\delta t_0 \tag{30}$$

where δt_0 and m are prescribed values (usually $m=8$, $\delta t_0=0.1$ days). Subscript s stands for the s-th time-step (inside the k-th phase). NS_k is the total number of time-steps inside the k-th phase. Times $t_{s,k}$ and $t_{s+1,k}$ are respectively the lower and upper bound of the s-th time-step (in particular $t_{1,k}=t_k$).

Adopting this method, at time $t=t_{s,k}$ the integral in the second term of the left-hand member of Eq. (27) may be written as follows:

$$\begin{cases}\displaystyle\int_{t_{1,k}}^{t_{s,k}}J(t_{s,k},\tau)d\underline{\psi}(z,\tau)=\sum_{n=1}^{s-1}\left\{\frac{\delta_k\underline{\psi}(z,t_{n+1,k})-\delta_k\underline{\psi}(z,t_{n,k})}{2}\cdot\sum_{g=1}^{2}[W_g\cdot J(t_{s,k},t_{ng,k})]\right\}\\ t_{ng,k}=\dfrac{1}{2}[a_g(t_{n+1,k}-t_{n,k})+t_{n+1,k}+t_{n,k}]\end{cases} \tag{31}$$

where a_g and W_g are respectively the abscissa (in the reference time-step from -1 to 1) and the weight factor of the g-th sampling point for Gaussian integration.

Substituting Eq. (31) into Eq. (27) finally gives:

$$\left[\underline{\underline{A}}(z) + \underline{\underline{B}}_s^{(k)}(z) \cdot \sum_{g=1}^{2} \frac{W_g \cdot J(t_{s,k}, t_{(s-1)g,k})}{2}\right] \cdot \delta_k \underline{\psi}(z, t_{s,k}) =$$

$$= \sum_{r=1}^{k} \{ \underline{\underline{B}}_c(z, t_{1,r}) \Delta_r \underline{\psi}(z) \cdot [J(t_{s,k}, t_{1,r}) - J(t_{1,k}, t_{1,r})] \} +$$

$$-\frac{1}{2} \cdot \sum_{r=1}^{k-1} \left[\underline{\underline{B}}_s^{(r)}(z) \cdot \sum_{n=1}^{NS_r} \left\{ [\delta_r \underline{\psi}(z, t_{n+1,r}) - \delta_r \underline{\psi}(z, t_{n,r})] \cdot \sum_{g=1}^{2} W_g \cdot [J(t_{s,k}, t_{ng,r}) - J(t_{1,k}, t_{ng,r})] \right\} \right] +$$

$$+\frac{1}{2} \cdot \sum_{r=1}^{k-1} \sum_{n=1}^{NS_r} \left\{ [\delta_r \underline{M}(z, t_{n+1,r}) - \delta_r \underline{M}(z, t_{n,r})] \cdot \sum_{g=1}^{2} W_g \cdot [J(t_{s,k}, t_{ng,r}) - J(t_{1,k}, t_{ng,r})] \right\} +$$

$$+\frac{1}{2} \cdot \sum_{n=1}^{s-1} \left\{ [\delta_k \underline{M}(z, t_{n+1,k}) - \delta_k \underline{M}(z, t_{n,k})] \cdot \sum_{g=1}^{2} W_g \cdot J(t_{s,k}, t_{ng,k}) \right\} +$$

$$-\underline{\underline{B}}_s^{(k)}(z) \cdot \sum_{n=1}^{s-2} \left\{ [\delta_k \underline{\psi}(z, t_{n+1,k}) - \delta_k \underline{\psi}(z, t_{n,k})] \cdot \sum_{g=1}^{2} \frac{W_g \cdot J(t_{s,k}, t_{ng,k})}{2} \right\} +$$

$$+ \underline{\underline{B}}_s^{(k)}(z) \cdot \sum_{g=1}^{2} \frac{[W_g \cdot J(t_{s,k}, t_{(s-1)g,k})]}{2} \cdot \delta_k \underline{\psi}(z, t_{(s-1),k}) \cdot [\underline{D}_{sh}(z, t_{s,k}) - \underline{D}_{sh}(z, t_{1,k})] \qquad (32)$$

This equation determines $\delta_k \underline{\psi}(z, t_{s,k})$ when the values $\delta_r \underline{\psi}(z, t_{n,r}) \forall r = 1, 2, \ldots, k, n = 1, 2, \ldots, s-1$ are known. The history of $\underline{\psi}(z, t)$ (that is of the strain inside the cross section) will therefore be determined by means of an incremental process that starts at time of first loading by computing $\Delta_1 \underline{\psi}(z)$ (according to Eq. (12)) and goes on by progressively determining $\delta_1 \underline{\psi}(z, t_{1,1})$, $\delta_1 \underline{\psi}(z, t_{2,1})$, up to $\delta_1 \underline{\psi}(z, t_{SN_1,1})$ (by means of Eq. (32)), then computes $\Delta_2 \underline{\psi}(z)$, and so on.

Once that $\delta_k \underline{\psi}(z, t_{s,k})$ is known, stresses in the steel elements can be easily determined by means of their constitutive laws:

$$\begin{aligned}
\delta_k \sigma_a(y, z, t_{s,k}) &= \underline{\rho}^T \cdot [\delta_k \underline{\psi}(z, t_{s,k}) - \delta_k \underline{\psi}(z, t_{s-1,k})] \cdot E_a + \delta_k \sigma_a(y, z, t_{s-1,k}) \\
\delta_k \sigma_{si}(z, t_{s,k}) &= \underline{\rho}_{si}^T \cdot [\delta_k \underline{\psi}(z, t_{s,k}) - \delta_k \underline{\psi}(z, t_{s-1,k})] \cdot E_s + \delta_k \sigma_{si}(z, t_{s-1,k}) \qquad (33) \\
\delta_k \sigma_{pj}(z, t_{s,k}) &= \underline{\rho}_{pj}^T \cdot [\delta_k \underline{\psi}(z, t_{s,k}) - \delta_k \underline{\psi}(z, t_{s-1,k})] \cdot E_p + \delta_k \sigma_{pj}(z, t_{s-1,k})
\end{aligned}$$

whereas the use of the constitutive law of concrete to determine the stress distribution in the concrete part would require the knowledge of the relaxation function whose analytical expression is generally unknown (and therefore should be evaluated by means of the solution of another Volterra integral equation). Nevertheless, this problem can be overcome because of assumptions 1 and 5. Because of assumption 5, the stress in concrete is a linear function of ordinate *y*. Therefore, when the stresses in steel are known the equilibrium Eq. (24) becomes:

$$\int_{A_c(z)} \underline{\rho} \cdot \underline{\rho}^T \cdot dA_c(z) \cdot d\sigma_c(y, z, \tau), \underline{\rho}^{T^{-1}} = d\underline{M}(z, \tau) - \underline{\underline{B}}_s^{(k)}(z) \cdot d\underline{\psi}(z, \tau) \qquad (34)$$

that, when rewritten in terms of finite increments, gives:

$$\delta_k \sigma_c(y, z, t_{s,k}) = \underline{\rho}^T \underline{\underline{A}}^{-1}(z) \cdot \{[\delta_k \underline{M}(z, t_{s,k}) - \delta_k \underline{M}(z, t_{s-1,k})] + - \underline{\underline{B}}_s^{(k)}(z) \cdot [\delta_k \underline{\psi}(z, t_{s,k}) - \delta_k \underline{\psi}(z, t_{s-1,k})]\} + \delta_k \sigma_c(y, z, t_{s-1,k}) \tag{35}$$

4. Structural analysis

As already stated, term $\delta_k \underline{M}(z, t_{s,k})$ in Eqs. (32) and (35) (related to the delayed variation $\delta\underline{\psi}$) and term $\Delta_r \underline{M}(z)$ in Eq. (29) (related to the instantaneous change $\Delta\underline{\psi}$) are unknowns owing to the redundancy of the structure. Structural analysis is therefore needed to determine these values.

Before discussing this topic a remark is necessary. The time-scale t previously adopted is the age of concrete in a cross section. When dealing with the overall behaviour of the bridge this time-scale does not apply any more because the age of the segments of the bridge is not the same. Therefore an absolute time-scale T, that is a time scale related to the construction phases, is necessary to determine the ages $t_{s,k}^d$ of each d-th segment of the bridge deck at absolute time $T_{s,k}$ (see Fig. 4). In the following, superscript d will be dropped to simplify the equations.

The redundant bending moments will be determined through the compatibility method (see for instance Mola 1993, 1999).

4.1 Relation between unknown redundant bending moments and internal actions

A straight beam continuous over Q_k spans is the static scheme adopted to perform structural analysis of the bridge deck. If L_q is the length of the q-th span and z is its longitudinal local axis (with origin in the left end of the span, see Fig. 5), the distribution of the bending moment inside the span is

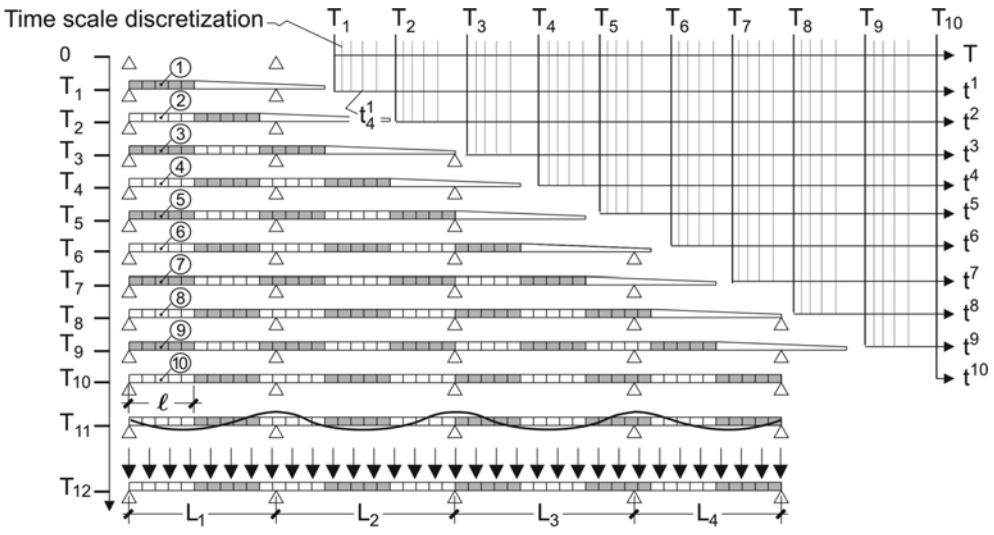

Fig. 4 Relation between the absolute time-scale T and local time scales t^d

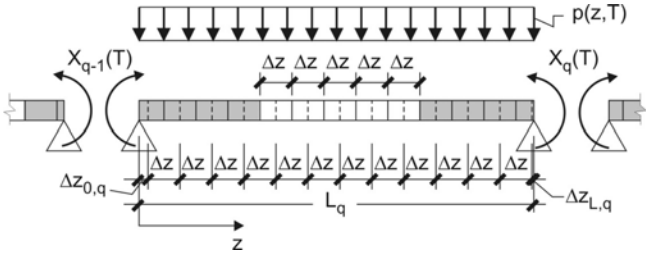

Fig. 5 Graphical description of the compatibility method at time T in the q-th span

$$\underline{M}(z, T) = \underline{M}_0(z, T) + \underline{\underline{M}}_1(z) \cdot \underline{X}_q(T) \qquad 0 \le z \le L_q \tag{36}$$

where $\underline{X}_q(T) = \left|X_{q-1}(T)\ X_q(T)\right|^T$ is the vector of the unknown redundant bending moments at the left and right end of the span,

$$\underline{\underline{M}}_1(z) = \begin{bmatrix} 0 & 0 \\ \dfrac{L_q - z}{L_q} & \dfrac{z}{L_q} \end{bmatrix} \tag{37}$$

and $\underline{M}_0(z, T)$ is the vector of the internal actions (axial force and bending moment) due to the external loads in a simply supported beam of length L_q. If the external load $p(z, T)$ is orthogonal to the beam axis, we immediately write

$$\underline{M}_0(z, T) = \begin{vmatrix} 0 \\ M_0(z, T) \end{vmatrix} = \left| \begin{matrix} 0 \\ \displaystyle\int_0^z \frac{L_q - z}{L_q} s \cdot p(s, T)ds + \int_z^{L_q} \left[\frac{L_q - z}{L_q} z - \frac{z}{L_q}(s - z)\right] \cdot p(s, T)ds \end{matrix} \right| \tag{38}$$

The partial derivative of Eq. (36), made with respect to time T is

$$\frac{\partial \underline{M}(z, T)}{\partial T} = \frac{\partial \underline{M}_0(z, T)}{\partial T} + \underline{\underline{M}}_X^{(q)}(z) \cdot \frac{d\underline{X}(T)}{dT} \qquad 0 \le z \le L_q \tag{39}$$

where vector $\underline{X}(T)$ is the vector that contains all the unknown redundant bending moments of the structure and

$$\underline{\underline{M}}_X^{(q)}(z) = \begin{array}{c} \begin{matrix} 1 & \dots & q-2 & q-1 & q & q+1 & \dots & Q_k - 1 \end{matrix} \\ \left| \begin{matrix} 0 & \dots & 0 & 0 & 0 & 0 & \dots & 0 \\ 0 & \dots & 0 & \dfrac{L_q - z}{L_q} & \dfrac{z}{L_q} & 0 & \dots & 0 \end{matrix} \right| \end{array} \tag{40}$$

If the external load $p(z, T)$ is constant all over the k-th phase, then $\partial p(z, T)/\partial T = 0$. Moreover, when replacing $d\underline{X}(T)/dT$ with an interpolation formula (namely a finite difference), Eq. (39) becomes:

$$\frac{\partial \underline{M}(z,T)}{\partial T} = \underline{\underline{M}}_X^{(q)}(z)\cdot\frac{d\,\underline{X}(T)}{dT} \cong \underline{\underline{M}}_X^{(q)}(z)\cdot\frac{\delta_k\underline{X}(T_{n+1,k})-\delta_k\underline{X}(T_{n,k})}{T_{n+1,k}-T_{n,k}} \Rightarrow \quad \begin{array}{l} 0\le z\le L_q \\ q=1,\ldots,Q_k \end{array}$$

$$\Rightarrow \delta_k\underline{M}(z,T_{n+1,k})-\delta_k\underline{M}(z,T_{n,k}) = \underline{\underline{M}}_X^{(q)}(z)\cdot[\delta_k\underline{X}(T_{n+1,k})-\delta_k\underline{X}(T_{n,k})] \quad T_{n,k}\le T\le T_{n+1,k} \tag{41}$$

Finally, substituting Eq. (41) into Eq. (32) one obtains

$$[\underline{\underline{\tilde{A}}}_1(z,t_{s,k})\,\vdots\,\underline{\underline{\tilde{A}}}_2(z,t_{s,k})]\times[\underline{Y}_1^T(z,t_{s,k})\,\vdots\,\underline{Y}_2^T(z,t_{s,k})]^T = \underline{\tilde{F}}(z,t_{s,k}) \tag{42}$$

where

$$\underline{\underline{\tilde{A}}}_1(z,t_{s,k}) = \left[\underline{\underline{A}}(z)+\underline{\underline{B}}_s^{(k)}(z)\cdot\sum_{g=1}^{2}\frac{W_g\cdot J(t_{s,k},t_{(s-1)g,k})}{2}\right]$$

$$\underline{\underline{\tilde{A}}}_2(z,t_{s,k}) = -\underline{\underline{M}}_X^{(q)}(z)\cdot\sum_{g=1}^{2}W_g\cdot\frac{J(t_{s,k},t_{(s-1)g,k})}{2}$$

$$\underline{Y}_1(z,t_{s,k}) = \delta_k\underline{\psi}(z,t_{s,k})$$

$$\underline{Y}_2(T_{s,k}) = \delta_k\underline{X}(T_{s,k}) \tag{43}$$

$$\underline{\tilde{F}}(z,t_{s,k}) = \sum_{r=1}^{k}\{\underline{\underline{B}}_c(z,t_{1,r})\Delta_r\underline{\psi}(z)\cdot[J(t_{s,k},t_{1,r})-J(t_{1,k},t_{1,r})]\}+$$

$$-\sum_{r=1}^{k-1}\left[\underline{\underline{B}}_s^{(r)}(z)\cdot\sum_{n=1}^{NS_r}\left\{[\delta_r\underline{\psi}(z,t_{n+1,r})-\delta_r\underline{\psi}(z,t_{n,r})]\cdot\sum_{g=1}^{2}W_g\cdot\frac{J(t_{s,k},t_{ng,r})-J(t_{1,k},t_{ng,r})}{2}\right\}\right]+$$

$$+\sum_{r=1}^{k-1}\sum_{n=1}^{NS_r}\left\{(\delta_r\underline{M}(z,t_{n+1,r})-\delta_r\underline{M}(z,t_{n,r}))\cdot\sum_{g=1}^{2}W_g\cdot\frac{J(t_{s,k},t_{ng,r})-J(t_{1,k},t_{ng,r})}{2}\right\}+$$

$$+\sum_{n=1}^{s-2}\left\{(\delta_k\underline{M}(z,t_{n+1,k})-\delta_k\underline{M}(z,t_{n,k}))\cdot\sum_{g=1}^{2}W_g\cdot\frac{J(t_{s,k},t_{ng,k})}{2}\right\}+$$

$$-\delta_k\underline{M}(z,T_{s-1,k})\cdot\sum_{g=1}^{2}W_g\cdot\frac{J(t_{s,k},t_{(s-1)g,k})}{2}+[\underline{D}_{sh}(z,t_{s,k})-\underline{D}_{sh}(z,t_{1,k})]+$$

$$-\underline{\underline{B}}_s^{(k)}(z)\cdot\sum_{n=1}^{s-2}\left\{[\delta_k\underline{\psi}(z,t_{n+1,k})-\delta_k\underline{\psi}(z,t_{n,k})]\cdot\sum_{g=1}^{2}W_g\cdot\frac{J(t_{s,k},t_{ng,k})}{2}\right\}+$$

$$+\underline{\underline{B}}_s^{(k)}(z)\cdot\delta_k\underline{\psi}(z,t_{(s-1),k})\cdot\sum_{g=1}^{2}W_g\cdot\frac{J(t_{s,k},t_{(s-1)g,k})}{2}$$

In Eq. (42), term $\delta_k\underline{M}(t_{s,k})$ is replaced by $\delta_k\underline{X}(T_{s,k})$, i.e., the unknown variation of the redundant bending moments at time $T_{s,k}$. In the last of Eqs. (43) $\delta_k\underline{M}(t_{n,k})$ is written as a function of the local time-scale of the cross-section because it is the bending moment inside that cross section at previous time $t_{n,k}$, when that section probably was located in another position inside the structure.

4.2 Compatibility equations

When applying the compatibility approach to the $Q_k - 1$ redundant bending moments, the compatibility conditions can be written as follows

$$\beta_{q,2}(T) + \beta_{q+1,1}(T) = 0 \qquad q = 1, 2, \ldots, Q_k - 1 \tag{44}$$

where $\beta_{q,2}(T)$ stands for the rotation of the right end (subscript 2) of the q-th span, and $\beta_{q+1,1}(T)$ is the rotation of left end (subscript 1) of the $(q+1)$-th span. The principle of virtual work allows these rotations to be written as a function of the curvatures over the q-th and $(q+1)$-th spans:

$$\beta_{q+1,1}(T) = \int_0^{L_{q+1}} \frac{L_{q+1} - z}{L_{q+1}} \cdot \chi(z, T)dz = \int_0^{L_{q+1}} M_1^*(z) \cdot \chi(z, T)dz$$

$$\beta_{q,2}(T) = \int_0^{L_q} \frac{z}{L_q} \cdot \chi(z, T)dz = \int_0^{L_q} M_2^*(z) \cdot \chi(z, T)dz \tag{45}$$

and therefore Eq. (44) becomes:

$$\int_0^{L_q} M_2^*(z) \cdot \chi(z, T)dz + \int_0^{L_{q+1}} M_1^*(z) \cdot \chi(z, T)dz = 0 \qquad q = 1, \ldots, Q_k - 1 \tag{46}$$

To evaluate the integrals in Eq. (46) the trapezoidal rule is applied. This is because this rule (and generally speaking all Newton-Côtes integration formulas) allows equidistant sampling points to be adopted. Each monolithic segment will therefore be subdivided into sub-segments of equal length Δz. The method herein discussed evaluates the stress and strain evolution inside all the midspan sections (named sampling sections) of each sub-segment of every monolithic segment of the bridge deck.

When adopting the trapezoidal rule, each term at the left side of Eq. (46) becomes:

$$\begin{aligned}\int_0^{L_\eta} M_\gamma^*(z) \cdot \chi(z, T)dz = &\left[\left(\frac{\Delta z_{0,\eta} \cdot \Delta z + \Delta z_{0,\eta}^2}{2\Delta z}\right) \cdot M_\gamma^*(0) + \left(\frac{\Delta z + \Delta z_{0,\eta}}{2}\right) \cdot M_\gamma^*(z_1)\right] \cdot \chi(z_1, t) + \\ &+ \left[\Delta z \cdot M_\gamma^*(z_2) - \frac{\Delta z_{0,\eta}^2}{2\Delta z} \cdot M_\gamma^*(0)\right] \cdot \chi(z_2, t) + \sum_{h=3}^{F_\eta - 2} [\Delta z \cdot M_\gamma^*(z_h)] \cdot \chi(z_h, t) + \\ &+ \left[\Delta z \cdot M_\gamma^*(z_{F_\eta - 1}) - \frac{\Delta z_{L,\eta}^2}{2\Delta z} \cdot M_\gamma^*(L_\eta)\right] \cdot \chi(z_{F_\eta - 1}, t) + \\ &+ \left[\left(\frac{\Delta z + \Delta z_{L,\eta}}{2}\right) \cdot M_\gamma^*(z_{F_\eta}) + \left(\frac{\Delta z_{L,\eta} \cdot \Delta z + \Delta z_{L,\eta}^2}{2\Delta z}\right) \cdot M_\gamma^*(L_\eta)\right] \cdot \chi(z_{F_\eta}, t)\end{aligned} \tag{47}$$

where $\gamma = 1$ and $\eta = q$ or $\gamma = 2$ and $\eta = q + 1$, depending on the term computed. $M_\gamma^*(z)$ is assigned in Eq. (45). F_η is the total number of sampling sections inside the η-th span at time T.

Note that $\Delta z_{0,\eta}$ represents the distance between the left end of the η-th span and the first sampling section inside the span, and $\Delta z_{L,\eta}$ stands for the distance between the last sampling section before the right end of the span and the nearest bearing. This because usually Δz is not a submultiple of the length of each span, but only of the length of the bridge (see Fig. 5). In this case a linear extrapolation made from the curvature in the two sampling sections of the span closest to its end

allows the curvature over the bearing to be evaluated.

Curvature $\chi(z_h, t)$ is written as a function of local age t of the section that actually is at abscissa z_h. Eq. (47) can be written in matrix form, that is

$$\int_0^{L_\eta} M_\gamma^*(z) \cdot \chi(z, T) dz = \sum_{h=1}^{F_\eta} C_{\gamma,\eta}[h] \cdot \chi(z_h, t) = \underline{\tilde{C}}_{\gamma,\eta}^T \cdot \underline{\Psi}(t) \tag{48}$$

and

$$\underline{\tilde{C}}_{\gamma,\eta}^T = [0 \;\; C_{\gamma,\eta}^1 \vdots 0 \;\; C_{\gamma,\eta}^2 \vdots \ldots \vdots 0 \;\; C_{\gamma,\eta}^{F_\eta}] \tag{49}$$

$$C_{\gamma,\eta}^1 = \left[\left(\frac{\Delta z_{0,\eta} \cdot \Delta z + \Delta z_{0,\eta}^2}{2\Delta z}\right) \cdot M_\gamma^*(0) + \left(\frac{\Delta z + \Delta z_{0,\eta}}{2}\right) \cdot M_\gamma^*(z_1)\right]$$

$$C_{\gamma,\eta}^2 = \left[\Delta z \cdot M_\gamma^*(z_2) - \frac{\Delta z_{0,\eta}^2}{2\Delta z} \cdot M_\gamma^*(0)\right]$$

$$C_{\gamma,\eta}^h = \Delta z \cdot M_\gamma^*(z_h) \qquad h = 3, \ldots, (F_\eta - 2) \tag{50}$$

$$C_{\gamma,\eta}^{F_\eta - 1} = \left[\Delta z \cdot M_\gamma^*(z_{F_\eta - 1}) - \frac{\Delta z_{L,\eta}^2}{2\Delta z} \cdot M_\gamma^*(L)\right]$$

$$C_{\gamma,\eta}^{F_\eta} = \left[\left(\frac{\Delta z + \Delta z_{L,\eta}}{2}\right) \cdot M_\gamma^*(z_{F_\eta}) + \left(\frac{\Delta z_{L,\eta} \cdot \Delta z + \Delta z_{L,\eta}^2}{2\Delta z}\right) \cdot M_\gamma^*(L)\right]$$

If $\underline{\Psi}(t)$ is the vector of the unknown terms $\underline{\psi}(z_h, t)$ inside the q-th span, i.e.,

$$\underline{\Psi}(T) = [\underline{\psi}^T(z_1, t) \vdots \underline{\psi}^T(z_2, t) \vdots \ldots \vdots \underline{\psi}^T(z_h, t) \vdots \ldots \vdots \underline{\psi}^T(z_{F_q}, t)]^T \tag{51}$$

when replacing Eq. (47) into Eq. (46), written in incremental form, one obtains

$$\underline{\tilde{C}}_{2,q}^T \cdot \delta_k \underline{\Psi}_q(T_{s,k}) + \underline{\tilde{C}}_{1,q+1}^T \cdot \delta_k \underline{\Psi}_{q+1}(T_{s,k}) = 0 \qquad q = 1, \ldots, Q_k - 1 \tag{52}$$

Eq. (52), because of the third of Eqs. (43), becomes

$$\begin{aligned} \underline{\tilde{Y}}_{1,q}(T_{s,k}) &= [\underline{Y}_1^T(z_{1,q}, t_{s,k}) \vdots \ldots \vdots \underline{Y}_1^T(z_{h,q}, t_{s,k}) \vdots \ldots \vdots \underline{Y}_1^T(z_{F_q,q}, t_{s,k})]^T = \\ &= [\delta_k \underline{\psi}^T(z_{1,q}, t_{s,k}) \vdots \ldots \vdots \delta_k \underline{\psi}^T(z_{h,q}, t_{s,k}) \vdots \ldots \vdots \delta_k \underline{\psi}^T(z_{F_q,q}, t_{s,k})]^T = \delta_k \underline{\Psi}_q(T_{s,k}) \end{aligned} \tag{53}$$

$$\underline{\tilde{C}}_{2,q}^T \cdot \underline{\tilde{Y}}_{1,q}(T_{s,k}) + \underline{\tilde{C}}_{1,q+1}^T \cdot \underline{\tilde{Y}}_{1,q+1}(T_{s,k}) = 0 \qquad q = 1, \ldots, Q_k - 1 \tag{54}$$

5. Overall analysis

The overall analysis of the structure consists in combining cross-section analysis with structural analysis.

5.1 Computation of the delayed variations $\delta_k \underline{\psi}$ and $\delta_k \underline{X}$

At time $T_{s,k}$ (s-th time-step inside the k-th phase) Eq. (42) can be written for every sampling section already cast, and Eq. (54) can be written for every redundant bending moment of the bridge deck. The solving system is the coupling of the equilibrium Eq. (42) and of the compatibility Eq. (54):

$$\left[\begin{array}{c|c} \tilde{\underline{\underline{D}}}_1(t_{s,k}) & \tilde{\underline{\underline{D}}}_2(t_{s,k}) \\ \hline \tilde{\underline{\underline{D}}}_3 & \underline{\underline{0}} \end{array}\right] \cdot \left[\begin{array}{c} \tilde{\underline{Y}}_{1,1}(T_{s,k}) \\ \tilde{\underline{Y}}_{1,2}(T_{s,k}) \\ \cdots \\ \tilde{\underline{Y}}_{1,Q_k}(T_{s,k}) \\ \hline \underline{Y}_2(T_{s,k}) \end{array}\right] = \left[\begin{array}{c} \tilde{\underline{G}}_1(t_{s,k}) \\ \tilde{\underline{G}}_2(t_{s,k}) \\ \cdots \\ \tilde{\underline{G}}_{Q_k}(t_{s,k}) \\ \hline \underline{0} \end{array}\right] \tag{55}$$

where Q_k is number of spans already casted at actual time $T_{s,k}$. The unknowns are terms $\delta_k \underline{\psi}(t_{s,k})$ of each sampling sections and the redundant bending moments $\delta_k \underline{X}(T_{s,k})$ (see the third and forth of Eqs. (43), as well as Eq. (53)).

Matrix $\tilde{\underline{\underline{D}}}_1(t_{s,k})$ is equal to

$$\tilde{\underline{\underline{D}}}_1(t_{s,k}) = \left[\begin{array}{cccc} \tilde{\underline{\underline{D}}}_{1,1}(t_{s,k}) & \underline{\underline{0}} & \cdots & \underline{\underline{0}} \\ \underline{\underline{0}} & \tilde{\underline{\underline{D}}}_{1,2}(t_{s,k}) & \cdots & \underline{\underline{0}} \\ \cdots & \cdots & \cdots & \cdots \\ \underline{\underline{0}} & \underline{\underline{0}} & \cdots & \tilde{\underline{\underline{D}}}_{1,Q_k}(t_{s,k}) \end{array}\right] \tag{56}$$

where

$$\tilde{\underline{\underline{D}}}_{1,q}(t_{s,k}) = \left[\begin{array}{cccc} \tilde{\underline{\underline{A}}}_1(z_{1,q}, t_{s,k}) & \underline{\underline{0}} & \cdots & \underline{\underline{0}} \\ \underline{\underline{0}} & \tilde{\underline{\underline{A}}}_1(z_{2,q}, t_{s,k}) & \cdots & \underline{\underline{0}} \\ \cdots & \cdots & \cdots & \cdots \\ \underline{\underline{0}} & \underline{\underline{0}} & \cdots & \tilde{\underline{\underline{A}}}_1(z_{F_q,q}, t_{s,k}) \end{array}\right] \quad q = 1, \ldots, Q_k \tag{57}$$

Terms $\tilde{\underline{\underline{A}}}_1(z_{h,q}, t_{s,k})$ in Eq. (57) have already been assigned in the first of Eqs. (43):

$$\tilde{\underline{\underline{A}}}_1(z_{h,q}, t_{s,k}) = \left[\underline{\underline{A}}(z_{h,q}) + \underline{\underline{B}}_s^{(k)}(z_{h,q}) \cdot \sum_{g=1}^{2} \frac{W_g \cdot J(t_{s,k}, t_{(s-1)g,k})}{2}\right] \quad \begin{array}{l} h = 1, \ldots, F_q \\ q = 1, \ldots, Q_k \end{array} \tag{58}$$

Matrix $\tilde{\underline{\underline{D}}}_2(t_{s,k})$ is equal to

$$\tilde{\underline{\underline{D}}}_2(t_{s,k}) = \left[\begin{array}{c} \tilde{\underline{\underline{D}}}_{2,1}(t_{s,k}) \\ \tilde{\underline{\underline{D}}}_{2,2}(t_{s,k}) \\ \cdots \\ \tilde{\underline{\underline{D}}}_{2,Q_k}(t_{s,k}) \end{array}\right] \tag{59}$$

where

$$\underline{\underline{\tilde{D}}}_{2,q}(t_{s,k}) = \begin{bmatrix} \underline{\underline{\tilde{A}}}_2(z_{1,q}, t_{s,k}) \\ \underline{\underline{\tilde{A}}}_2(z_{2,q}, t_{s,k}) \\ \cdots \\ \underline{\underline{\tilde{A}}}_2(z_{F_q,q}, t_{s,k}) \end{bmatrix} \qquad q = 1, \ldots, Q_k \tag{60}$$

Terms $\underline{\underline{\tilde{A}}}_2(z_{h,q}, t_{s,k})$ in Eq. (60) have already been assigned in the second of Eqs. (43):

$$\underline{\underline{\tilde{A}}}_2(z_{h,q}, t_{s,k}) = -\underline{\underline{M}}_X^{(q)}(z_{h,q}) \cdot \sum_{g=1}^{2} W_g \cdot \frac{J(t_{s,k}, t_{ng,k})}{2} \qquad \begin{matrix} h = 1, \ldots, F_q \\ q = 1, \ldots, Q_k \end{matrix} \tag{61}$$

where terms $\underline{\underline{M}}_X^{(q)}(z_{h,q})$ are computed in Eq. (40).

Matrix $\underline{\underline{\tilde{D}}}_3$ is equal to

$$\underline{\underline{\tilde{D}}}_3 = \begin{bmatrix} \underline{\tilde{C}}_{2,1}^T & \underline{\tilde{C}}_{1,2}^T & \underline{0} & \underline{0} & \cdots & \underline{0} & \underline{0} \\ \underline{0} & \underline{\tilde{C}}_{2,2}^T & \underline{\tilde{C}}_{1,3}^T & \underline{0} & \cdots & \underline{0} & \underline{0} \\ \underline{0} & \underline{0} & \underline{\tilde{C}}_{2,3}^T & \underline{\tilde{C}}_{1,4}^T & \cdots & \underline{0} & \underline{0} \\ \cdots & \cdots & \cdots & \cdots & \cdots & \cdots & \cdots \\ \underline{0} & \underline{0} & \underline{0} & \underline{0} & \cdots & \underline{\tilde{C}}_{1,Q_k-1}^T & \underline{0} \\ \underline{0} & \underline{0} & \underline{0} & \underline{0} & \cdots & \underline{\tilde{C}}_{2,Q_k-1}^T & \underline{\tilde{C}}_{1,Q_k}^T \end{bmatrix} \tag{62}$$

where terms $\underline{\tilde{C}}_{\gamma,\eta}$ are the vectors already assigned in Eqs. (49) and (50). The number of rows in matrix $\underline{\underline{\tilde{D}}}_3$ is equal to the actual number of redundant bending moments in the structure.

Finally

$$\underline{\tilde{G}}_q(t_{s,k}) = [\underline{\tilde{F}}^T(z_{1,q}, t_{s,k}) \quad \underline{\tilde{F}}^T(z_{2,q}, t_{s,k}) \quad \ldots \quad \underline{\tilde{F}}^T(z_{F_q,q}, t_{s,k})]^T \qquad q = 1, \ldots, Q_k \tag{63}$$

where vectors $\underline{\tilde{F}}^T(z_{h,q}, t_{s,k})$ are those already shown in the last of Eqs. (43).

Obviously, during launching phases the number of unknowns grows together with the structure.

In this analysis the launching nose is the first segment of the bridge deck. The only difference with respect to the other segments is that this segment has a distinct length and is a steel structure. Therefore it can be taken into account by means of the equations already stated.

5.2 Computation of the instantaneous variations $\Delta_k \underline{\psi}$ and $\Delta_k \underline{X}$ at the beginning of the k-th phase

The instantaneous changes $\Delta_k \underline{\psi}$ and $\Delta_k \underline{X}$ are caused by:

1) launching forward one segment length with hydraulic jacks
2) service prestressing (carried out upon completion of the launch)
3) application of the load due to blanket, sidewalks, parapets and railings

In all these cases the system to be solved consists of the equilibrium equations of all the sampling sections and of the compatibility equations that are necessary to perform the structural analysis. Nevertheless, in this case Eq. (32) is replaced by Eq. (12), making the system much simpler.

Case b) refers to the condition $\Delta \underline{\overline{P}}_k \neq \underline{0}$ whereas cases a) and c) imply that $\Delta \underline{\overline{P}}_k = \underline{0}$. When dealing with case a) it has to be pointed out that the structure changes: a new monolithic segment is added and the deck (that is all the sampling sections already cast) slides forward. In this case the superposition principle does not apply.

If time t_k^- is the instant immediately before launch, then vectors $\underline{\psi}(z_{h,q}, t_k^-)$ and $\underline{M}(z_{h,q}, t_k^-)$ are known. In particular, vector $\underline{\psi}(z_{h,q}, t_k^-)$ is the sum of the elastic response $\underline{\psi}_e(z_{h,q}, t_k^-)$ plus the effect of the delayed behaviour of concrete $\underline{\psi}^*(z_{h,q}, t_k^-)$ (its effect is similar to that of a thermal strain), i.e.,

$$\underline{\psi}(z_{h,q}, t_k^-) = \underline{\psi}_e(z_{h,q}, t_k^-) + \underline{\psi}^*(z_{h,q}, t_k^-) \tag{64}$$

The effect of launch is instantaneous and can be interpreted as the release of the deck already cast from the supports followed by its placing over the bearings in the new position. Therefore (see Eq. (12))

$$\underline{\psi}_e(z_{h,q}, t_k^-) = [\underline{\underline{B}}_c(z_{h,q}, t_k^-) + \underline{\underline{B}}_s^{(k-1)}(z_{h,q})]^{-1} \cdot \underline{M}(z_{h,q}, t_k^-) \qquad \begin{matrix} h = 1, \ldots, F_q \\ q = 1, \ldots, Q_k \end{matrix} \tag{65}$$

At time t_k immediately after launch Eq. (64) can be written as follows:

$$\underline{\psi}(z_{h,q}, t_k) = \underline{\psi}_e(z_{h,q}, t_k) + \underline{\psi}^*(z_{h,q}, t_k^-) \tag{66}$$

Therefore Eq. (12) becomes

$$\begin{aligned} &[\underline{\underline{B}}_c(\overline{z}_{h,q}, t_k) + \underline{\underline{B}}_s^{(k)}(\overline{z}_{h,q})] \cdot [\underline{\psi}_e(z_{h,q}, t_k) + \underline{\psi}^*(z_{h,q}, t_k^-)] = \\ &= \underline{M}(\overline{z}_{h,q}, t_k) + [\underline{\underline{B}}_c(\overline{z}_{h,q}, t_k) + \underline{\underline{B}}_s^{(k)}(\overline{z}_{h,q})] \cdot \underline{\psi}^*(z_{h,q}, t_k^-) \end{aligned} \tag{67}$$

that is

$$[\underline{\underline{B}}_c(\overline{z}_{h,q}, t_k) + \underline{\underline{B}}_s^{(k)}(\overline{z}_{h,q})] \cdot \underline{\psi}(\overline{z}_{h,q}, t_k) = \underline{M}(\overline{z}_{h,q}, t_k) - \underline{M}_T^*(\overline{z}_{h,q}, t_k) \tag{68}$$

where $\underline{M}_T^*(\overline{z}_{h,q}, t_k)$ is known.

Note that this computation can be repeated more than once while the deck is sliding toward its new position (a sampling section moves from $z_{h,q}$ to $\overline{z}_{h,q}$), so that stresses and strains can be accurately evaluated during launch.

To conclude, when dealing with case c) Eq. (12) has to be replaced by Eqs. (65), (66) and (68).

5.3 Computation of the displacements

The computation of the transverse displacement v of the structure could be performed by means of a direct double numerical integration of the curvatures in all the sampling sections, by means of shape functions, by means of the adoption of the finite difference method or by means of the

application of the principle of virtual work. The principle of virtual work is the method adopted because it involves a simple and recurrent equation for every sampling section already cast, at any time step. The integral over z axis is performed by means of the trapezoidal rule.

6. Examples

The first example is a comparison of two elastic solutions. This example shows the efficiency of the trapezoidal rule to perform integration over the deck longitudinal axis. The structure is a two span beam, prestressed with a straight tendon whose eccentricity with respect to the centre of gravity of the cross section is y_p. In Fig. 6 the exact solution for the instantaneous redundant bending moment over the central support (that is $X = \frac{3}{2}E_p A_p \overline{\varepsilon}_p y_p$) is compared with the outcome of the proposed algorithm. When adopting 20 sampling sections per span, the error is only 0.12%.

The second example compares two visco-elastic solutions. This example tests the reliability of the

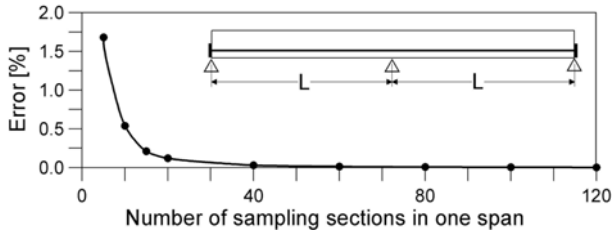

Fig. 6 Variation of the error gathered with the number of sampling sections

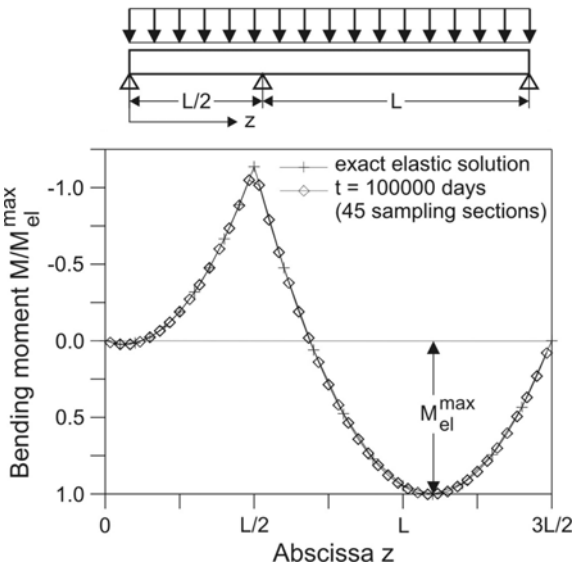

Fig. 7 Comparison of the bending moments along the beam

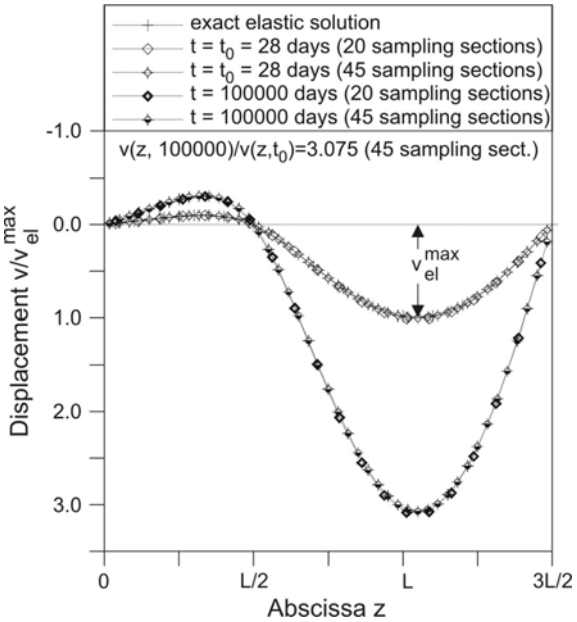

Fig. 8 Displacements along the beam

Gauss formula to perform the Volterra integrals. The homogeneous visco-elastic beam, cast in one single phase, is shown in Fig. 7. Because of the first theorem of linear visco-elasticity, stresses inside the beam do not change whereas transverse displacements v vary according to $v(z, t) = v(z, t_0) \cdot [1 + \varphi(t, t_0)] = v_{el}(z) \cdot [1 + \varphi(t, t_0)]$.

Fig. 7 shows that the bending moments computed by the computer program at time $t = 100000$ days are exactly the same of the elastic solution. It was assumed that $\varphi(100000, t_0) = 2.075$. The calculated displacement shown in Fig. 8 satisfies the requirements of the first theorem of linear viscoelasticity.

The third and last example deals with a launched bridge. The bridge involves six inner spans with length $L = 37.5$ m and two side spans with $L = 30$ m for a total length $L_T = 285$ m. The launching nose is 30.25 m long. The bridge has been built with segments 37.5 m long, each one launched six days after casting. The casting operations have been scheduled every seven days as one day was required for placing the steel cage and preparing the formwork.

The basic data for concrete are: characteristic cylindrical compressive strength $f_{ck} = 50$ MPa; elastic modulus at 28 days $E_{c28} = 38.6$ GPa; final creep coefficient $\varphi(\infty, 6) = 1.65$ according to the CEB-FIP Model Code 90 (CEB 1991). Regarding steel we have: characteristic tensile strength $f_{ptk} = 1800$ MPa; characteristic tensile stress at 0.1% of residual deformation $f_{pk}(0.1) = 1620$ MPa; elastic modulus $E_p = 195$ GPa.

The prestressing steel ratio for the straight tendons is 0.27% while for the service prestressing tendons the steel ratio is 0.17%.

In Fig. 9 the bending moment X_1 is reported versus time. The abrupt changes are related to the instant of launch, while the smooth lines describe the structural relaxation. Furthermore, the values of the bending moment are higher in comparison with the elastic ones. This behaviour can be explained by remembering that during launching the vertical displacement of the metallic nose increases in time owing to concrete creep. Consequently, the imposed displacement that is applied to the bridge front edge when the steel nose reaches the support is higher in comparison with the

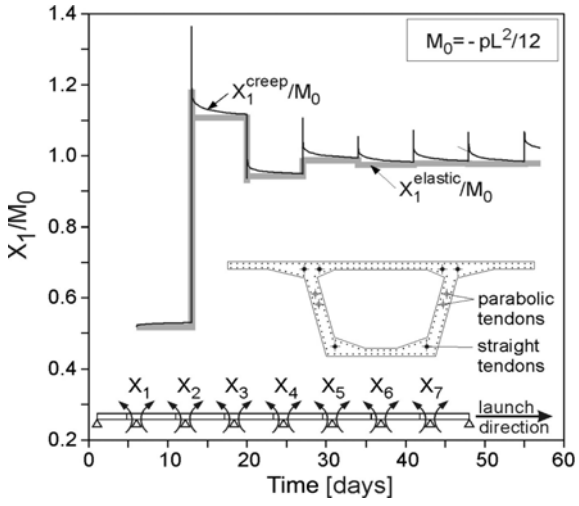

Fig. 9 Bending moment X_1 during the concreting phases

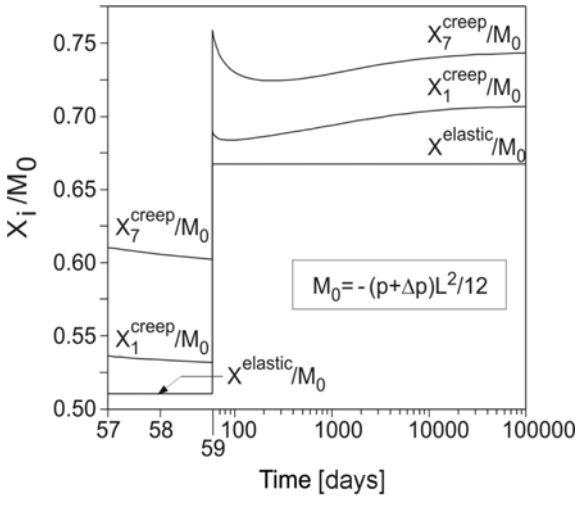

Fig. 10 Redundant bending moments in the service stage

one which would be applied when considering an elastic behaviour of the structure. The instantaneous bending moments induced in the continuous beam are therefore higher than those computed discarding creep of concrete. Even though these moments reduce their values according to concrete relaxation, they remain higher than the elastic ones.

Fig. 10 is related to the long term behaviour of the bridge in its final configuration including the effects of the service prestressing, applied at $T = 57$ days, and the ones connected to the permanent overloading (load due to blanket, sidewalks, parapets and railings), applied at $T = 59$ days. It can be observed that the elastic behaviour does not vary in time and exhibits bending moments which are about 6% and 11% lower than the ones evaluated taking into account creep effects.

The application of the service prestressing modifies the distribution of the bending moments by introducing parasitic effects. The time variation of these effects is produced by two distinct factors, namely the reduction of the prestressing force in the cables and the variation of the moment distribution consequent to the rheological nonhomogeneity of the continuous beam. The reduction of the prestressing force induces a reduction of the parasitic effects whereas the rheological nonhomogeneity increases them.

Fig. 10 shows that the redundant moments (induced by the service prestressing together with all the previous history) are reducing in time, so we can conclude that the reduction of the prestressing force governs the structural response.

Finally, it can be observed that in the service stage (that is for $T > 59$ days), the relative increase of moment X_1 is higher in comparison with the analogous of moment X_7. In particular it results $X_1(\infty)/X_1(59) > 1$, $X_7(\infty)/X_7(59) < 1$. Moreover, for $59 \le T \le \sim 200$ days X_7 decreases with time increase. The same behaviour affects X_1 in the restricted interval $59 \le T \le \sim 100$. The elastic increase of the bending moments X_7 induced by the permanent overloading is nearly equal to that of X_1, as it is influenced only by the nonhomogeneous distribution of the elastic modulus. On the contrary, the increase in time of the bending moments due to creep is rather marked. Therefore, the reduction generated by the relaxation under application of the imposed displacement when the metallic nose reaches the last support (which is more pronounced for X_7 than for X_1 because the front spans of the bridge are more aged) is overcome after a certain time interval. This aspect is clearly shown in

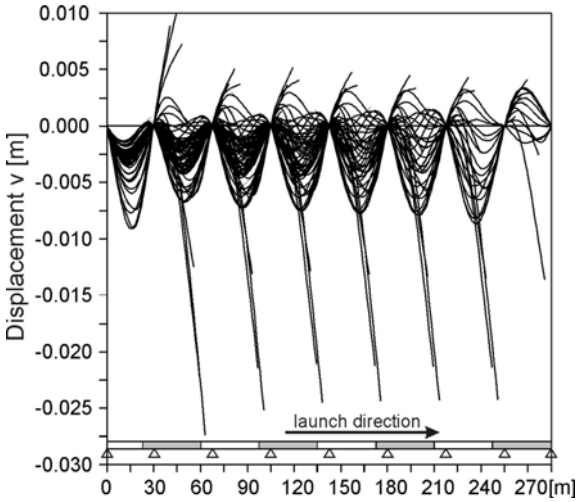

Fig. 11 Transverse displacements envelope during the launching phases

Fig. 10 where the curves describing the development in time of moments X_1 and X_7 increase.

Displacements larger than those related to the final configuration are present during the construction process as shown by Fig. 11, in which the envelope of the transverse displacements during the construction process has been reported. It can be observed that the maximum displacements are downwards and are about three times larger than the upwards ones. The deflexion of the nose edge is initially upwards when the bridge is composed by only one span and it rapidly goes down reaching its maximum downwards value when the nose edge is near the third support.

The envelope of the alternate deflections maintains its basic properties in every span except for the last in which the presence of the previous spans reduces the related displacements.

7. Conclusions

The launching technique represents a feasible method for the construction of prestressed concrete bridges and nowadays it has been successfully applied in many outstanding cases.

When adopting this construction method, prestressing can be conveniently calibrated, because of its subdivision in two different steps. In the first step the most feasible choice consists in introducing an axial centric prestressing by means of straight cables. In the second step, when the bridge has reached its final configuration, additional curved cables can be tensioned in order to counteract the bending moments due to permanent overloading and to variable loads.

The elastic analysis of launched bridges shows that in the construction phases particular care has to be devoted in computing the stresses in the two spans behind the advancing front of the bridge. Nevertheless, the construction process has no practical influence on the structural response in the service stage, so that the main problem regards the correct dimensioning of the metallic nose in terms of relative length, weight and stiffness.

When approaching the design of launched bridges in a more refined way the elastic analysis reveals itself unable to correctly predict the structural behaviour, as during the launching process not negligible delayed deformations due to concrete creep take place. Consequently, the vertical displacements imposed to the advancing edge of the beam when it reaches a support are higher than the ones that can be computed by means of an elastic analysis. As the most part of the creep deformations are not reversible, the imposed displacements are inelastic in a large extent and so the initial value of the bending moments related to them is relaxed in time, remaining however higher than the value computed assuming an elastic behaviour of the structure. After completion of the bridge deck, the time variation of its moment distribution is connected to the rheological nonhomogeneity of the structure and to the variation of the effects due to service prestressing.

The most important effects due to creep develop in the launching phase, for which a refined analysis of the sequence of loads and imposed displacements has to be performed. The procedure discussed in the paper allows the problem to be correctly solved and the outcomes show that not negligible inaccuracies can be introduced if the analysis is limited to the elastic domain.

It is noteworthy to observe that the sequence of loads, imposed deformations, prestressing and distribution of the rheological nonhomogeneities configure a very complex time-dependent problem which cannot be satisfactory investigated by recurring to the simplified methods of creep structural analysis. Therefore, the proposed procedure, even though quite complex from the computational point of view, represents the only way of reaching reliable results.

References

Baur, W. (1977), "Bridge erection by launching is fast, safe, and efficient", *J. Civil Eng.*, ASCE, March 1977, 60-63.

Bazant, Z.P. (1975), "Theory of creep and shrinkage in concrete structures: A precise of recent developments", *Mechanics Today*, **2**.

CEB (1984), *Manual on Structural Effects of Time-dependent Behaviour of Concrete*, CEB Bulletin n.142/142 Bis, Georgi Publishing Co., Saint Saphorin, Switzerland.

CEB (1991), *CEB-FIP Model Code 1990*, CEB Bulletin d'Information n. 203/204/205, CEB, Lausanne, Switzerland.

Eibl, J. (1995), *Concrete Structures Euro-design Handbook*, Ernst & Sohn, Berlin.

Favre, R. and Laurencet, P. (1999), "Pont poussé à géométrie complexe. Cas des viaducts de l'Île Falcon en Suisse", *Travaux*, **754**, 57-64.

Ghali, A. and Favre, R. (1986), *Concrete Structures: Stresses and Deformations*, Chapman and Hall, New York.

Grant, A. (1975), "Incremental launching of concrete structures", *ACI J.*, August 1975, 395-402.

Göhler, B. and Pearson, B. (2000), *Incrementally Launched Bridges*, Ernst & Sohn, Berlin.

Hewson, N. (2003), *Prestressed Concrete Bridges: Design and Construction*, Thomas Telford Ltd.

Leonhardt, F. (1973), "Procédé de construction par cycles de bétonnage en coffrage fixe et cycles de poussage", *Annales de l'Institut Technique du Batiment et des Travaux Publics, No. 301, serie: Travaux Publics n. 153*, 45-63.

Libby, J.R. (1984), *Modern Prestressed Concrete*, Van Nostrand Reinhold Company Inc., New York.

Mc Henry, D. (1943), "A new aspect of creep in concrete and its application to design", *Proc. ASTM*, **43**.

Mola, F. (1986), "General analysis of non homogeneous viscoelastic sections and structures" (in Italian), *Studi e Ricerche*, Italcementi, Bergamo, Italy, **8**, 119-198.

Mola, F. (1993), "The reduced relaxation function method: An innovative approach to creep analysis of non homogeneous structures", *Int. Conf. on Concrete & Structures*, Hong Kong, March 16-17, 149-156.

Mola, F. (1999), "A general approach to long-term analysis of concrete structures and its application in engineering practice", *3rd Int. Conf.: Analytical Models and New Concepts in Mechanics of Concrete Structures*, Wroclaw, Poland, June 16-19, 195-198.

Mola, F. and Pisani, M.A. (1993), "Creep analysis of non-homogeneous concrete structures", *Creep and Shrinkage of Concrete*, Edited by Z.P. Bazant and I. Carol, Published by E & FN Spon, London, 597-602.

Pisani, M.A. (1994), "Numerical analysis of creep problems", *Comput. Struct.*, **51**(1), 57-63.

Rosignoli, M. (1998), *Launched Bridges*, ASCE Press, Reston, VA.

Rosignoli, M. (1999), "Prestressing schemes for incrementally launched bridges", *J. Bridge Eng.*, **4**(2), 107-115.

Rosignoli, M. (2000), "Thrust and guide devices for launched bridges", *J. Bridge Eng.*, **5**(1), 75-83.

Sasmal, S., Ramanjaneyulu, K., Srinivas, V. and Gopalakrishnan, S. (2004), "Simplified computational methodology for analysis and studies on behaviour of incrementally launched continuous bridges", *Struct. Eng. Mech.*, **17**(2), 245-266.